2019 IEEE/RSJ International Conference on Intelligent Robots and Systems (IROS)
Macau, China, November 4-8, 2019

3D Micromanipulation of Particle Swarm Using a Hexapole Magnetic Tweezer

Xiao Zhang, Louis William Rogowski, and Min Jun Kim

Abstract— **This article discusses the design, modeling, and application of a powerful hexapole magnetic tweezer system for closed-loop 3D swarm control applications. The system consists of six sharp tapered magnetic poles that are integrated with six electromagnetic coils and mounted on two yokes composed of 3D printed magnetic material. Magnetic field gradients are generated at the sharp tips of the magnetic poles when current is applied through the attached electromagnetic coils. Different combinations of current input can interact with magnetized microparticles to create three-dimensional motion. A closed-loop control algorithm based on image processing and hardware integration through MATLAB was developed to automatically operate external power supplies connected to the magnetic tweezer system. Coordinate system transformation is utilized to transform the tilted actuation coordinates, by virtue of the system hardware configuration, to the measurement coordinates used during experiments and analysis. This magnetic tweezer system has the advantage of a larger working space and higher magnetic field strengths when compared to several other similar designs. The magnetic tweezer system allows for more diverse applications within the microscale, such as microparticle swarm control, cell penetration, and cell therapy. Experimental analysis performed in this article demonstrates the closed-loop navigation of a microparticle swarm moving freely in both 2D and 3D environments. Results show highly consistent trajectories within the swarm with only a few fluctuations due to microflows. This system will keep being updated and optimized to investigate the performance of microparticles in *in vivo* environments.**

I. INTRODUCTION

Microscale robotics has been widely investigated due to their huge potential in numerous applications, such as drug delivery[1-3], micromanipulation[4, 5], noninvasive surgery and DNA topology studies[6-9]. As a necessary step towards deploying microrobots for these applications, the control and navigation of microrobot swarms towards a target location is not only required, but fundamental, to future research, especially for circumstances that require bulk payload to be transported wirelessly. A common method to produce microrobot manipulation is to apply an external force or torque on the microrobot; the microrobot is often pre-composed of a specific size or shape to enable actuation. There are several prevalent ways to actuate such microrobots, such as using mechanical force, optical force, thermal expansion, magnetic torque and magnetic gradient force. Different manipulation systems have been developed based on those principles, including atomic force microscopy (AFM)[3], optical tweezer systems[10, 11], a permanent magnetic stage system[12], electromagnetic coil systems[13, 14] and magnetic tweezer systems[15], all of which have been widely used for microscale research, DNA analysis, and cell studies [11, 15-18]. AFM is one of the most popular applications in micro and nanoscale research for its ability to take measurements and perform experimental analysis with high degrees of accuracy. However, the AFM mechanism requires its probe to have close contact with the sample, and can be heavily influenced by environmental factors such as vibration, electrical noise, and temperature, thus making it unsuitable for swarm manipulation of microrobots, especially when indirect contact is necessary[3]. Optical tweezer systems utilize highly focused laser beams to generate an attractive or repulsive force that varies based on the relative refractive index between the sample and its surrounding environment. The generated force is usually in a piconewton magnitude, while the system resolution is normally low and requires high power to operate. When it comes to *in vivo* environments, more difficulties occur, as the optical tweezer cannot precisely distinguish between the surrounding environment and the target of interest[10, 11]. The permanent magnetic stage system is equipped with a strong neodymium permanent magnet connected to servo motors; this system can control either a single microrobot or a swarm of them in a 2D plane, however the ability to navigate in the z direction is currently limited, since the system has restricted controllability on both the direction and magnitude of the applied force[12]. Rotating magnetic fields are mainly used in electromagnetic coil systems to interact with microrobots such that magnetic torques are generated for microrobot propulsion; the propulsion direction is often normal to the plane of rotation[13, 14, 19, 20]. However, the interaction for creating propulsion through magnetic torques requires the microrobot's structure to be either flexible[21] (soft body, i.e.) or have chirality (helical form, i.e.)[20]. The transformation from rotating magnetic torques into actual swimming motion is more complex than the other methods, due to uncertainties involving the shape, rigidity, and magnetism of the microrobot itself, along with environmental effects inherent to the fluidic medium. This can be highly unpleasant if the given task needs to manipulate a microrobot swarm to perform an operation, like drug delivery, that requires microrobots to transport pharmaceuticals to the same target location and having microrobots respond uniformly to the same globally applied inputs. A magnetic tweezer system contains several magnetic

*Research supported by National Science Foundation.

Xiao Zhang is with the Department of Mechanical Engineering, Southern Methodist University, Dallas, TX 75275, U.S.A. (email: xiaozhang@smu.edu).

Louis William Rogowski is with the Department of Mechanical Engineering, Southern Methodist University, Dallas, TX 75275, U.S.A. (email: lrogowski@smu.edu).

Min Jun Kim is with the Department of Mechanical Engineering, Southern Methodist University, Dallas, TX 75275, U.S.A. (email: mjkim@lyle.smu.edu).

978-1-7281-4004-9/19/$31.00 ©2019 IEEE

poles acting as terminals to release magnetic field fluxes and produce magnetic field gradients in the working space. When current is applied to the related electromagnetic coil on the poles, the gradient field then interacts with magnetized microrobots to generate magnetic force for propulsion[8, 15-18, 22-26]. The drawback of this system is that the produced gradient field strength decays drastically as the distance from the pole tips to the sample increases[22, 27, 28]. However, this can be mitigated by increasing either the number of turns in the attached coils or by increasing the input current. The nature of a magnetic tweezer system simply requires microrobots to be magnetized instead of having a specific structure or rigidity[29]. The magnetic field gradients only affect magnetized objects, which brings advantages to applications in *in vivo* environments, as the biological substances are mostly non-magnetized[8, 30]. As shown in the earlier work[16, 31], our system setup shows higher performance than some other designs developed by different research groups[15, 17, 22-28], enabling us to perform swarm control tasks and other experiments in a larger working space with a higher power input. It is for these advantages that more research needs to be conducted, both to understand the capabilities offered by this magnetic tweezer system and how viable swarm control is for future applications.

In the experiments shown in this paper, we mainly focus on swarm control of magnetic microparticles instead of manipulating an individual microrobot. The magnetic gradients are applied uniformly through the sample area, allowing for uniform control. Since no specific microrobot shape is necessary for actuation using the magnetic tweezer, simple magnetic microparticles can be utilized to perform swarm navigation. The microparticles are directed to perform arbitrary trajectories in both 2D and 3D planes of motion. The 2D and 3D planes of motion were then compared against each other in terms of performance, taking into account of drag forces, microflows, and other experimental factors. We also demonstrate the accuracy of a *z*-focal plane estimation technique to track the 3D motion of the microparticles. All of this demonstrates the consistency of similar microparticles under the same control input and helps move us towards a more feasible method of 3D closed-loop feedback control. This article is presented as follows: Section II reveals the hardware design and control modeling of our magnetic tweezer system, which illustrate the system setup, closed-loop control mechanism and the force generation mechanism. Section III discusses the experimental results and analysis of 2D and 3D motion and swarm control of microparticles and the conclusions are in Section IV.

II. DESIGN AND MODELLING

A. Hardware Design and Fabrication

The CAD design shown in Fig. 1 illustrates the components of the magnetic tweezer system. Two hexagonal yokes, which were 3D printed with Proto-pasta Magnetic Iron PLA material (0.15 T magnetic saturation), are positioned as a double-layer structure. Each yoke has an outer and inner perimeter of 133.1 mm and 82.3 mm, respectively. When current is applied to the system, the two yokes form a closed magnetic circuit to reduce the excitation current needed for creating a magnetic field and decreases the amount of heat generated by the system, such that the fluidic medium of interest is unaffected. [15-17]. A total of six magnetic poles with sharp tips[16] (40 μm in diameter) were made of cobalt iron alloy (high magnetic saturation of 2.35 T, VACOFLUX 50, VACUUMSCHMELZE GmbH & Co.KG) material through laser cutting (Polaris Laser Laminations, LLC) and then installed on the top and bottom yokes. The tips are pointed towards the center of the working space with the vertical distance between poles on the top and bottom planes being 2.040 mm. Each of the three poles on the same yoke has a gap of 3.668 mm between the other two. The overall effective working space located in the center of the system is 2 mm × 2 mm × 0.5 mm as shown in [15]. At the end of each magnetic pole, an electromagnetic coil with 527 turns of AWG-25 heavy-built insulated copper wire generates the magnetic field flux when applied with an input current, which is then concentrated and released from the sharp tip of the pole to produce strong magnetic field gradient field. By positioning the poles correctly, a Cartesian system is formed for actuation, which is marked as the solid lines $X_aY_aZ_a$ in Fig. 1. The

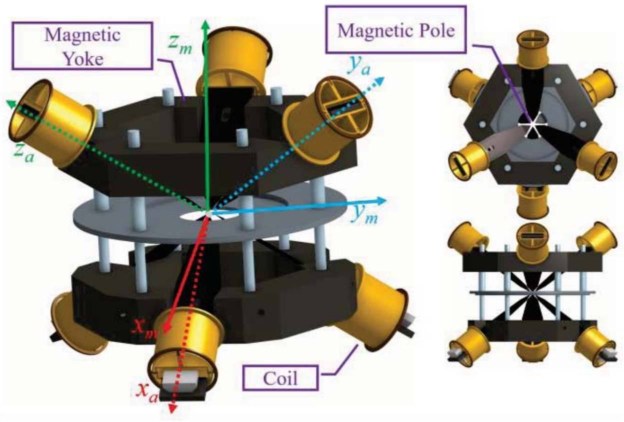

Fig. 1. CAD design of a magnetic tweezer system, the actuation coordinate system and measurement coordinate system are shown as solid and dashed lines, respectively. Each component of magnetic tweezer is marked as well. The sample is placed at the epicenter of the system, supporting a maximum sample size of 2 mm × 2mm × 0.5 mm.

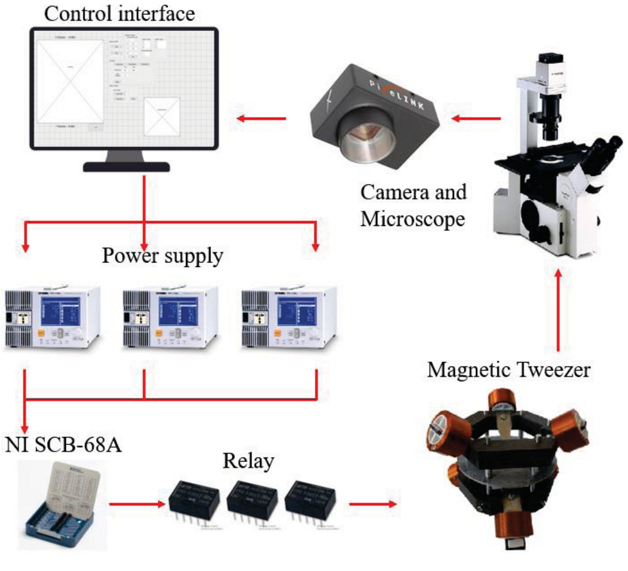

Fig. 2. Hardware integration of a magnetic tweezer system, red arrows indicate the control signal flow between each component.

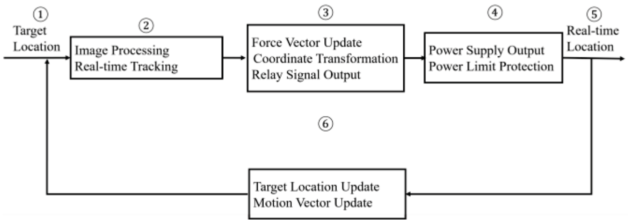

Fig. 3. Closed-loop control flow chart of a magnetic tweezer system.

measurement coordinate system $X_mY_mZ_m$, shown as a dash lines, is then acquired using the coordinate system transformation to enable the system to collect data in a more convenient way. The angles between each coordinate axis is as follows: X_a and X_m is 35.26°, Y_a and Y_m is 45°, Z_a and Z_m is 54.74°. All the coordinate information shown in the images and data analysis contained within this paper are consistent with the measurement coordinate system shown in Fig. 1.

The assembled magnetic tweezer was then integrated with the rest of the external system components (CCD camera, power supplies, computer programming with MATLAB, etc.) to establish the complete system as illustrated in Fig. 2. Red arrows indicate the data flow directions of the control signals between each component. The visual acquisition and image processing are performed using a Pixelink D734CU-T color camera, which is configured to 2048 × 2048 resolution with 3 frames per second (fps), mounted on an Olympus IX50 microscope with a 40× objective. The relatively low fps is mainly due to the high resolution, which is essential for wide fields of view. The real-time experiment images are delivered to the computer for closed-loop control after image processing and analysis. A National Instrument SCB-68A connector block and three AXICOM D3023 Relays are connected to the computer and three GW Instek programmable digital AC/DC power supplies to deliver current to the specific coil in each pair, thereby generating an arbitrary magnetic field gradient. There is one power supply for each pair of coils on the magnetic tweezer system, as discussed in [15], the magnetic field gradient under the activation of single magnetic pole can be as high as 0.8 T/m.

B. Modelling and Experimental Setup

The magnetic field flux density $\boldsymbol{B}$ is calculated from Eq. (1)-(2) [22], however, in our system, the six poles are not connected to the same yoke as in [22], so the matrix $\boldsymbol{K_I}$ in magnetic charge matrix $\boldsymbol{Q}$ can be neglected. Additionally, only 3 poles will be activated at the same time, so the matrix $\boldsymbol{Q} = [q_1\ q_2\ q_3]^{\mathrm{T}}$. $\Re_a$ is the reluctance between pole tip and working space center. N_c indicates the total turns of each coil, μ_0 is the permeability of medium in the working space (air), q_i is the magnetic charge defined by $q_i = \Phi/\mu_0$, where Φ is the magnetic flux, r_i is the distance from the magnetic pole to microparticle. All of the above is then multiplied with $\boldsymbol{u_i}$, the normalized direction vector from the magnetic pole to the microparticle in order to get the magnetic flux density.

$$\boldsymbol{Q} = \frac{N_c}{\mu_0 \Re_a}\boldsymbol{I_f} \tag{1}$$

$$\boldsymbol{B} = \sum_{i=1}^{3}\frac{4\pi}{\mu_0}\frac{q_i}{r_i^2}\boldsymbol{u_i} \tag{2}$$

The swarm of microparticles reaches a stable velocity quickly during the experiment, which means a force balance is also reached between the attraction force $\boldsymbol{F_{magnetic}}$ and the resistance force $\boldsymbol{F_{viscous}}$; using modified Stoke's law[7, 32] in Eq. (3), we can calculate the viscous drag force by analyzing the velocity profile of microparticles to obtain the magnetic force:

$$\boldsymbol{F_{magnetic}} = \boldsymbol{F_{viscous}} = 6\pi\eta r\boldsymbol{v}(1+\frac{9r}{16h}) \tag{3}$$

η is the viscosity of the sample solution, r is the radius of the microparticle and $\boldsymbol{v}$ represents its velocity profile, h is the distance between centriod of microparticle and the sample chamber wall. The ratio of h to r is so large that the last term becomes insignificant and can be ignored. Also, the magnitudes of the gravitational force and the buoyancy force are around the same level and are negligible when compared to the magnetic force, espeically if the size of the microparticle is very small[33]. For microparticles with same material but of different geometric sizes, the larger ones will generate a higher magnetic force due to a greater magnetic dipole.

$$\begin{aligned} {}^{a}_{m}\boldsymbol{R} &= [R_x(45°)][R_y(35.26°)] \\ &= \begin{bmatrix} 0.8165 & 0 & -0.5774 \\ 0.4082 & 0.7071 & 0.5774 \\ 0.4082 & -0.7071 & 0.5774 \end{bmatrix} \end{aligned} \tag{4}$$

$$\boldsymbol{X_a} = \begin{bmatrix} x_a \\ y_a \\ z_a \end{bmatrix} = {}^{a}_{m}\boldsymbol{R} \cdot \begin{bmatrix} x_m \\ y_m \\ z_m \end{bmatrix} = {}^{a}_{m}\boldsymbol{R} \cdot \boldsymbol{X_m} \tag{5}$$

$$\boldsymbol{K_c} = \begin{bmatrix} K_{cx} \\ K_{cy} \\ k_{cz} \end{bmatrix}, \boldsymbol{I_f} = \begin{bmatrix} I_x \\ I_y \\ I_y \end{bmatrix} = K_g \cdot \boldsymbol{\hat{X}_a} + \boldsymbol{K_c} \tag{6}$$

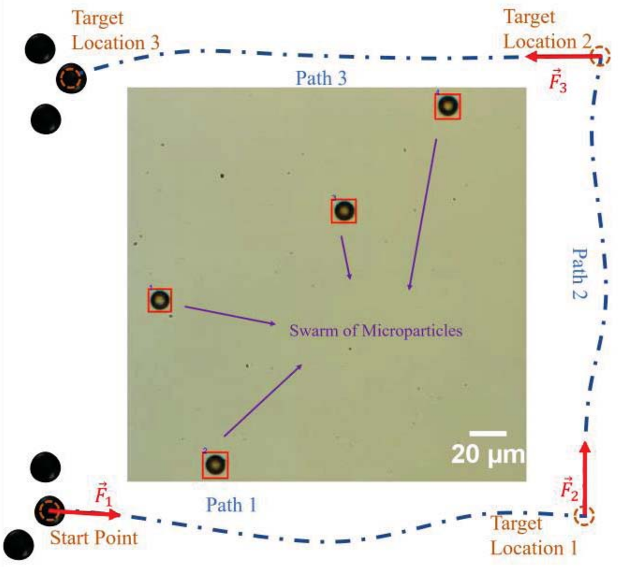

Fig. 4. Swarm control experiment overview. The swarm of microparticles departed from the start point, where the force vectors $\vec{F}_i$ are updated according to the given target location. Central figure shows the detail of a real-time experiment image, all detected microparticles are enclosed in red box with index number to record their coordinates information. The swarm is then guided to a series of arbitrary target coordinates that can be set by the user in all three dimensions.

Using a MATLAB graphical user interface module, the closed-loop control algorithm was developed as shown in the flow chart in Fig. 3, which explains the basic functions of the hardware and software integration. The target location is set by the user at the beginning of the experiment and transferred to the control program. Simultaneousy, the real-time experiment image is captured from the camera and processed to track all the single-bead microparticles with equal or similar size for consideration as a member of the swarm, so that they can show approximate behaviors. Due to the limited ability to directily assess z-axis changes using the camera, an indirect method of calculating the relative microparticle area size difference of different focal planes was deployed to record the z-coordinate of each microparticle[15, 34, 35]. In other words, as the centroid area of the particle changes with focal planes, we can infer how far it has traveled in the z direciton. Once the current has been applied to the coils and the target location is determined, the direction and force vector are calculated using Eq. (4)-(6). This firstly transforms the force vector from the measurement coordinates to the actuation coordinates. The obtained vector is then normalized to $\hat{\boldsymbol{X}}_a$, and multiplied afterwards by K_g, the amplifying factor that is given to ensure the maximum power output, and adds the compensation vector $\boldsymbol{K}_c = [0.04\ 0.01\ 0.01]^T$ that was determined from experimental calibration by trial and error to compensate for the pole tip deviations. Finally, we get the current vector $\boldsymbol{I}_f$ at the end of this process.

The sign of each component in $\boldsymbol{I}_f$ is recognized and sent to a relay that switches the current direction so that the power can be transmitted to the correct coil in each pole pair. The current vector is constantly updated during the experiment until microparticles reach the target area. Additionally, a power output limit is predefined to protect the coils and circuit from overheating, preventing hardware destruction. An experiment log containing microparticle location, power output, and other experimental parameters is recorded and stored after each experiment.

The sample is prepared by mixing magnetic particles (Spherotech SVFM-100-4 ferromagnetic particles, with average diameter of 10.6 μm and magnetic saturation of around 0.8 T) and deionized water to produce an 1% w/v particle concentration, it was then vortexed for 30 seconds and left on a permanent magnet for 15 seconds for magnetization. The experimental chamber is made from polydimethylsiloxane (PDMS) as a cylindrical shape with dimension of 5 mm in diameter and 1 mm in height. To decrease the surface friction of microparticles close to the substrate, a 20% concentration of Tween 20 solution was also introduced into the sample medium. The experiment sketch in Fig. 4 shows the overview of microparticle swarm control process described in the modelling part. A swarm of microparticles is detected in the working space at the starting point and marked by image processing and a tracking module. The power supplies provide a controlled power output to generate the specific force vector correlated to the target locations unitil microparticles reach to that position. On the way to the target, Brownian motion and microflow will constantly affect the motion of the swarm, but the control algorithm will continuously self-correct the force vector to assure the microparticles continue moving in the right direction. Finally they end up in the final target location and process is completed.

III. EXPERIMENT AND ANALYSIS

Microparticle swarm control using the magnetic tweezer system was proceeded by selecting one of the microparticles in the swarm and navigating it through the working space. As the properties such as size, weight and magnetization of the microparticles were almost identical, they will show similar behaviors under the same magnetic gradient field, though there still exist deviations due to the uncertainties within the fluid medium. For each test, three microparticles were selected and their trajectories were marked in three different line colors. The 3D swarm control trajectories in 3D view were also generated to represent the thorough motion of each microparticle. For each experiment shown below, the steered microparticle usually started on the bottom of the substrate unless specifically mentioned, while the other two may not have started on the same focal plane.

A. 2D Swarm Control and Analysis

The total size of field of view from the camera is 278 × 278 μm^2 on x-y plane, with a trackable z-direction of about 30 μm. Some of the microparticles are not on the same focal plane throughout the experiment, however, the magnetic field gradients act as uniform inputs within the working space[15]. Fig. 5 shows the 2D swarm control result of navigating a microparticle swarm to follow specific patterns of 'L', 'o', 'v' and 'e'. This was chosen in honor of Valentine's day. The target locations in each pattern were set such that the turning points were on the x-y plane and the z-component was equal to zero. The control power input was set such that it does not exceed 1.5 A in each power supply, this value was determined from experiments in earlier work to prevent the temperature in the working space from overheating as well as providing

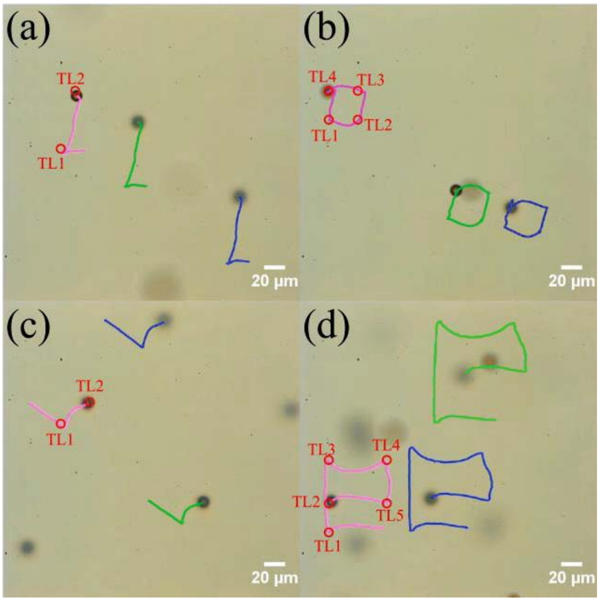

Fig. 5. 2D swarm control trajectory of 'Love' in (a)-(d). The finishing time for each pattern is 59 s, 80 s, 24 s and 166 s, respectively. 'TL' refers to target location. All particles were able to perform similar trajectories, with deviations resulting from internal flows or height differences in the sample.

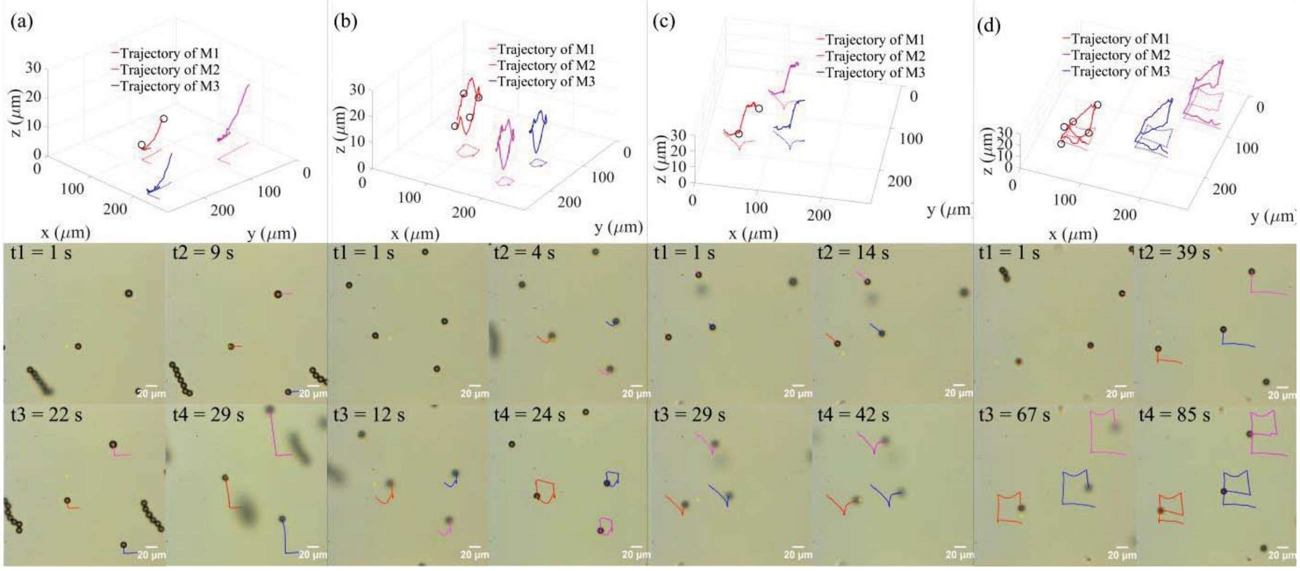

Fig. 6. 3D swarm control trajectory of 'Love' in (a)-(d) with 3D trajectory plots above each of them. Below each 3D plot are four images that show the stepwise procedure for making each trajectory. Black circles shown in each 3D trajectory are the target locations at each step. The projection of each trajectory is shown on the bottom of the *x-y* plane in each 3D plot. 'M1'- 'M3' refers to microparticles 1-3, the trajectory colors in 3D view figures are consistent with the experimental image representing them below. All time steps are related by t1, t2, t3 and t4 respectively.

enough power to allow microparticles to move at a suitable speed.

The swarm of microparticles in pattern 'L' shows excellent uniformity as all three microparticles have nearly identical routes, which indicates the existence of stable fluid environment and uniform magnetic force generated within the working space. In pattern 'o', most of the trajectories are in good shape, where the only obvious difference is at the end of the navigation, where the magenta microparticle went through its original location and moved to the right for a short distance, while the green one stopped exactly at its starting point and the blue one experienced insufficient motion to reach to the final point; by inspecting the top and bottom paths of each of them, it is apparent that the blue microparticle had a longer travel distance moving from left to right (TL1 to TL2 in magenta microparticle), which was quite possibly caused by a microflow that pushed it to the right and delayed it from moving to the left. The overall routes in letter 'v' are also in good shape, but one thing that should be noted is that the blue microparticle's path is slightly longer than the other two, this is due to the density profile along *z* direction in the medium; tween 20 solution has higher density and naturally sinks to the bottom of the sample, resulting in higher drag force within that area. Because the blue microparticle is in a higher position than the other two microparticles, and experiencing an equal amount of magnetic force, we can infer that its velocity is faster than those located in the lower layer according to Eq. (3). For pattern 'e', the magenta microparticle is the lowest and the green microparticle is the highest in terms of depth; the difference in height again reflects the trajectory shape difference. The trajectory length of the green microparticle has the longest path followed by the blue and magenta microparticle trajectories in decreasing length. However, all trajectories still form the distinctive pattern on control level, and this heterogeneity of velocity profile depending on the depth of microparticles in the swarm can be utilized in future more complex control tasks. The closed-loop control performance in 2D always showed good navigation and could manipulate a microparticle swarm through a desired pattern.

B. 3D Swarm Control and Analysis

The closed-loop control circumstance in 3D has more complexity than in the 2D case, this is caused by the appearance of *z*-direction motion. Also, Brownian motion, combined with the existence of random microflows, leads to a very unstable surrounding environment that can affect the movement of microparticles significantly. The same maximum current output of 1.5 A was also applied to the experiments in 3D. The recorded video frames and relevant 3D trajectory analysis are shown in Fig. 6, in which the target locations are labelled as black circles.

The movement of 'L' was set to moving to $z = 5$ µm at the corner and then going up to $z = 10$ µm. The selected microparticle in the swarm was at first slightly higher than 5 µm, but it dropped down around that height while also approaching the target *x-y* coordinates, the other two followed the same trend and showed similar motion. The magenta microparticle had a relatively longer path in 'L' due to the higher starting point and larger particle size, all the trajectories were smooth and stable as shown in the 3D view plot Fig. 6 (a). In trajectory 'o', the influence of an unstable microflow emerged. The starting point of the chosen microparticle was at 10 µm level with the rest in the swarm below it. When the first target location, with $z = 15$ µm (left-bottom corner on *x-y* plane), was reached, the swarm had some fluctuations but soon was stabilized and then headed to the next desired point with $z = 20$ µm. The third target point was on the same level with the second one, and the swarm reached to as high as 26 µm at the half way point, but then lowered to the expected point, from where it then set off to the original point at the 10 µm level. We can clearly see that red microparticle surpass the other two in total route length as it started in a higher position, the swarm could proceed to the preset points even though there were disturbances on the way. Pattern 'v' has comparative simplicity with ‘L’, in the experimental data; all three individuals in the swarm started from the bottom plane. The first desired point was at $z = 5$ μm, to lead the microparticle moving to the bottom center in Fig. 6(c). The swarm then navigated to the height of 20 μm. The final motion was waving up and down but the microparticles all ended up between 22 to 24 μm in the z-direction, each of the trajectories had almost same length as shown in t4 = 42 s in Fig. 6(c). Letter ‘e’ was the most complicated pattern to achieve as it had the most turns on the route with longest length. The first two target locations were on the plane of $z = 0$ μm. The swarm was then guided to the height of 20 μm directly to the upper-left corner. The rest of the trajectories were stable and showed the swarm of microparticles passing through the last two target points at $z = 10$ μm. The whole movement has better performance than the one displayed in ‘o’ as there was no drastic bouncing motion, fluctuations only happened at the beginning of the operation.

According to Fig. 5 and Fig. 6, it is apparent that less time was used in 3D swarm control to produce similar patterns than those in 2D under same power output restriction. This was caused by the lack of drag force far from the surface; however, the 2D motion had the benefit of having a steadier trajectory. The performance of x-y plane motion in both assignments can be considered satisfactory, and swarms can reach to the designated height within acceptable error range of less than 4 μm.

IV. CONCLUSION

This paper illustrated the design, modeling, experiment and analysis of a hexagonal magnetic tweezer system for closed-loop 2D/3D swarm control of magnetic microparticles. The integration of hardware and software was explained along with the illustration of the magnetic gradient field and force generation mechanism. The demonstration was proceeded by showing experiments involving microparticle swarm control in both 2D and 3D manners. 3D views of microparticle swarm motion trajectories were created using a focal plane area analysis of the microparticles and were displayed alongside real-time experimental data. This work has major benefits for swarm control related tasks, showing that not only can similar microparticles act homogeneously under a uniform input, but can also be reliably actuated to perform arbitrary 3D motion. While there were some issues with internal flows and fluidic heterogeneity, the microparticle swarms performed quite well in achieving their desired trajectories. Furthermore, the results guided future development of control systems for microrobotics and advance towards practically controllable magnetically actuated microparticles in *in vivo* environment for drug delivery and cell therapy applications.

ACKNOWLEDGMENT

This work was supported by the National Science Foundation (CMMI 1712096 and IIS 1712088).

REFERENCES

1. Dogangil, G., Ergeneman, O., Abbott, J.J., Pané, S., Hall, H., Muntwyler, S., and Nelson, B.J. *Toward targeted retinal drug delivery with wireless magnetic microrobots*. in *2008 IEEE/RSJ International Conference on Intelligent Robots and Systems*. 2008. IEEE.
2. Fusco, S., Chatzipirpiridis, G., Sivaraman, K.M., Ergeneman, O., Nelson, B.J., and Pané, S., *Chitosan electrodeposition for microrobotic drug delivery.* Advanced healthcare materials, 2013. **2**(7): p. 1037-1044.
3. Ferreira, A., Agnus, J., Chaillet, N., and Breguet, J.-M., *A smart microrobot on chip: Design, identification, and control.* IEEE/ASME Transactions on mechatronics, 2004. **9**(3): p. 508-519.
4. Steager, E.B., Sakar, M.S., Kim, D.H., Kumar, V., Pappas, G.J., and Kim, M.J., *Electrokinetic and optical control of bacterial microrobots.* Journal of Micromechanics and Microengineering, 2011. **21**(3): p. 035001.
5. Sakar, M.S., Steager, E.B., Kim, D.H., Kim, M.J., Pappas, G.J., and Kumar, V., *Single cell manipulation using ferromagnetic composite microtransporters.* Applied physics letters, 2010. **96**(4): p. 043705.
6. Kei Cheang, U., Lee, K., Julius, A.A., and Kim, M.J., *Multiple-robot drug delivery strategy through coordinated teams of microswimmers.* Applied physics letters, 2014. **105**(8): p. 083705.
7. Chiou, C.-H., Huang, Y.-Y., Chiang, M.-H., Lee, H.-H., and Lee, G.-B., *New magnetic tweezers for investigation of the mechanical properties of single DNA molecules.* Nanotechnology, 2006. **17**(5): p. 1217.
8. Haber, C. and Wirtz, D., *Magnetic tweezers for DNA micromanipulation.* Review of Scientific Instruments, 2000. **71**(12): p. 4561-4570.
9. Yan, J., Skoko, D., and Marko, J.F., *Near-field-magnetic-tweezer manipulation of single DNA molecules.* Physical Review E, 2004. **70**(1): p. 011905.
10. Wright, G.D., Arlt, J., Poon, W.C., and Read, N.D., *Optical tweezer micromanipulation of filamentous fungi.* Fungal Genetics and Biology, 2007. **44**(1): p. 1-13.
11. Neuman, K.C. and Nagy, A., *Single-molecule force spectroscopy: optical tweezers, magnetic tweezers and atomic force microscopy.* Nature methods, 2008. **5**(6): p. 491-505.
12. Sheckman, S., Kim, H., Manzoor, S., Rogowski, L.W., Huang, L., Zhang, X., Becker, A.T., and Kim, M.J. *Manipulation and control of microrobots using a novel permanent magnet stage*. in *2017 14th International Conference on Ubiquitous Robots and Ambient Intelligence (URAI)*. 2017. IEEE.
13. Cheang, U.K., Dejan, M., Choi, J., and Kim, M. *Towards Model-Based. Control Of Achiral Microswimmers*. in *The ASME Dynamic Systems and Control Conference*. 2014. American Society of Mechanical Engineers.
14. Cheang, U.K., Kim, H., Milutinović, D., Choi, J., Rogowski, L., and Kim, M.J. *Feedback control of three-bead achiral robotic microswimmers*. in *Ubiquitous Robots and Ambient Intelligence (URAI), 2015 12th International Conference on*. 2015. IEEE.
15. Zhang, X., Kim, H., and Kim, M.J., *Design, Implementation, and Analysis of a 3-D Magnetic Tweezer System With High Magnetic Field Gradient.* IEEE Transactions on Instrumentation and Measurement, 2019. **68**(3): p. 680-687.
16. Zhang, X., Kim, H., Rogowski, L.W., Sheckman, S., and Kim, M.J. *Novel 3D magnetic tweezer system for microswimmer manipulations*. in *Ubiquitous Robots and Ambient Intelligence (URAI), 2017 14th International Conference*. 2017. IEEE.
17. Zhang, Z., Huang, K., and Menq, C.-H., *Design, implementation, and force modeling of quadrupole magnetic tweezers.* IEEE/ASME Transactions on Mechatronics, 2010. **15**(5): p. 704-713.
18. Kummer, M.P., Abbott, J.J., Kratochvil, B.E., Borer, R., Sengul, A., and Nelson, B.J., *OctoMag: An electromagnetic system for 5-DOF wireless micromanipulation.* IEEE Transactions on Robotics, 2010. **26**(6): p. 1006-1017.
19. Cheang, U.K., Roy, D., Lee, J.H., and Kim, M.J., *Fabrication and magnetic control of bacteria-inspired robotic microswimmers.* Applied Physics Letters, 2010. **97**(21): p. 213704.
20. Cheang, U.K., Meshkati, F., Kim, D., Kim, M.J., and Fu, H.C., *Minimal geometric requirements for micropropulsion via magnetic rotation.* Physical Review E, 2014. **90**(3): p. 033007.
21. Ye, Z., Régnier, S., and Sitti, M., *Rotating magnetic miniature swimming robots with multiple flexible flagella.* IEEE Transactions on Robotics, 2014. **30**(1): p. 3-13.
22. Zhang, Z. and Menq, C.-H., *Design and modeling of a 3-D magnetic actuator for magnetic microbead manipulation.* IEEE/ASME Transactions on Mechatronics, 2011. **16**(3): p. 421-430.
23. Hosu, B.G., Jakab, K., Bánki, P., Tóth, F.I., and Forgacs, G., *Magnetic tweezers for intracellular applications.* Review of Scientific Instruments, 2003. **74**(9): p. 4158-4163.
24. Chen, L., Offenhäusser, A., and Krause, H.-J., *Magnetic tweezers with high permeability electromagnets for fast actuation of magnetic beads.* Review of Scientific Instruments, 2015. **86**(4): p. 044701.
25. Gosse, C. and Croquette, V., *Magnetic tweezers: micromanipulation and force measurement at the molecular level.* Biophysical journal, 2002. **82**(6): p. 3314-3329.
26. Chang, L., Howdyshell, M., Liao, W.C., Chiang, C.L., Gallego-Perez, D., Yang, Z., Lu, W., Byrd, J.C., Muthusamy, N., and Lee, L.J., *Magnetic Tweezers - Based 3D Microchannel Electroporation for High-Throughput Gene Transfection in Living Cells.* Small, 2015. **11**(15): p. 1818-1828.
27. Amblard, F., Yurke, B., Pargellis, A., and Leibler, S., *A magnetic manipulator for studying local rheology and micromechanical properties of biological systems.* Review of Scientific Instruments, 1996. **67**(3): p. 818-827.
28. Niu, F., Ma, W., Li, X., Chu, H.K., Yang, J., Ji, H., and Sun, D. *Modeling and development of a magnetically actuated system for micro-particle manipulation*. in *Nanotechnology (IEEE-NANO), 2014 IEEE 14th International Conference on*. 2014. IEEE.
29. Purcell, E.M., *Life at low Reynolds number.* American journal of physics, 1977. **45**(1): p. 3-11.
30. Bausch, A.R., Möller, W., and Sackmann, E., *Measurement of local viscoelasticity and forces in living cells by magnetic tweezers.* Biophysical journal, 1999. **76**(1): p. 573-579.
31. Zhang, X., Kim, H., Rogowski, L.W., Sheckman, S., and JunKim, M. *Development and Implementation of High Power Hexapole Magnetic Tweezer System for Micromanipulations*. in *2018 IEEE International Conference on Robotics and Automation (ICRA)*. 2018. IEEE.
32. Happel, J. and Brenner, H., *Low Reynolds number hydrodynamics: with special applications to particulate media*. Vol. 1. 2012: Springer Science & Business Media.
33. Wang, X., Luo, M., Ho, C., Zhang, Z., Zhao, Q., Dai, C., and Sun, Y. *Robotic Intracellular Manipulation: 3D Navigation and Measurement Inside a Single Cell*. in *2018 IEEE International Conference on Robotics and Automation (ICRA)*. 2018. IEEE.
34. Wu, M., Roberts, J.W., Kim, S., Koch, D.L., and DeLisa, M.P., *Collective bacterial dynamics revealed using a three-dimensional population-scale defocused particle tracking technique.* Applied and environmental microbiology, 2006. **72**(7): p. 4987-4994.
35. Wu, M., Roberts, J.W., and Buckley, M., *Three-dimensional fluorescent particle tracking at micron-scale using a single camera.* Experiments in Fluids, 2005. **38**(4): p. 461-465.